CrossMark
click for updates

Orientation of a dielectric rod near a planar electrode

Bas W. Kwaadgras,*[a] Thijs H. Besseling,[a] Tim J. Coopmans,[a] Anke Kuijk,[a] Arnout Imhof,[a] Alfons van Blaaderen,[a] Marjolein Dijkstra[a] and René van Roij[b]

We present experimental and theoretical results on suspensions of silica rods in DMSO–water, subjected to an applied electric field. The experimental results indicate that, if the electrode used for generating the electric field is in direct contact with the suspension, a fraction of the rods close to the electrode surface does not stand parallel to the field but instead lies flat on the electrode when the field is switched on. To explain these results theoretically, we modify the coupled dipole method to include "image dipoles", and find that a rod close to the electrode experiences not only the expected global potential energy minimum at an orientation parallel to the electric field, but also a local minimum several times the thermal energy in depth for orientations parallel to the electrode surface. Additionally, we indicate how the magnitude of the potential energy depends on the electric field strength and include results not only for negatively polarizable (which correspond to the aforementioned experimental system), but also for positively polarizable rods.

1 Introduction

Manipulation of colloidal dispersions with applied electric fields is a research subject with important technological applications. By polarization of the particles, an electric field introduces not only a preferred orientation for anisotropic particles, but also interparticle interactions that can allow the particles to assemble into ordered structures.[1] In this way, one can "switch on" order in a system by switching on an electric field, and switch off the order by switching off the electric field and allowing Brownian motion to destroy the ordered structure. For this reason, the subject receives a large amount of attention nowadays, both from the experimental[2–9] as well as the simulational[10–14] perspective.

Recently, a synthesis strategy for fluorescent silica rods was developed in our group by Kuijk *et al.*,[15,16] and the bulk phase behavior of these particles,[17] as well as their behavior in an external electric field was studied.[18,19] One finding that we will concentrate on in this work is that if the suspension of silica rods is in direct contact with the electrode used to generate the electric field, a fraction of the rods will, once the electric field is turned on, lie flat on the electrode while the others stand up straight, with no intermediate orientations observed. The flat-lying rods are still able to move and rotate freely in-plane with the electrode surface, which opens the perspective of creating an experimental two-dimensional system of silica rods, which is left for future work.

In this paper, we concentrate on the experimental finding itself and its theoretical explanation, which is based on the so-called coupled dipole method (CDM).[20–28] In this work, we will modify the CDM to allow for "image dipoles", in analogy with image charges.

2 Experiment

Two systems of fluorescent rod-like silica particles were synthesized according to the method of Kuijk *et al.*[15,16] The first system consisted of particles with an average length $l = 3.6$ μm ($\delta = 11\%$) and diameter $d = 660$ nm ($\delta = 11\%$), with δ the polydispersity (standard deviation over the mean). These particles had a gradient of fluorescein isothiocyanate (FITC) dye along their main axis.[16] Fig. 1(a) shows a transmission electron microscopy (TEM) image of the particles. The second system consisted of particles with an average length $l = 3.3$ μm ($\delta = 10\%$) and diameter $d = 550$ nm ($\delta = 11\%$). These particles were fluorescently labeled with an FITC-dyed shell. Both particle systems were dispersed in an index-matching mixture ($n_D^{21} = 1.45$) of 10 : 1 mass ratio dimethylsulfoxide (DMSO) and ultrapure water.[15]

To apply an electric field to the suspended particles, sample cells were built with two conductive indium tin oxide (ITO)-coated glass coverslips (30–60 Ω, Diamond Coatings) functioning as electrodes. The two electrodes were on the inside of the cell, in direct contact with the suspension, as shown in Fig. 1(b). They were separated by either glass coverslip spacers (No. 0, Menzel Gläzer) or a thin layer of UV-glue (Norland No. 68), which resulted in a separation of approximately 100 μm and 15 μm respectively. Thermocouple alloy wires (diameter 50 μm, Goodfellow) were connected to the ITO layers with silverpaint (SPI-paint). The ends

[a] *Debye Institute for Nanomaterials Science, Utrecht University, Princetonplein 5, 3584 CC Utrecht, The Netherlands. E-mail: baskwaadgras@gmail.com; Tel: +31 30 253 2952*

[b] *Institute for Theoretical Physics, Center for Extreme Matter and Emergent Phenomena, Utrecht University, Leuvenlaan 4, 3584 CE Utrecht, The Netherlands. E-mail: r.vanroij@uu.nl; Tel: +31 30 253 7479*
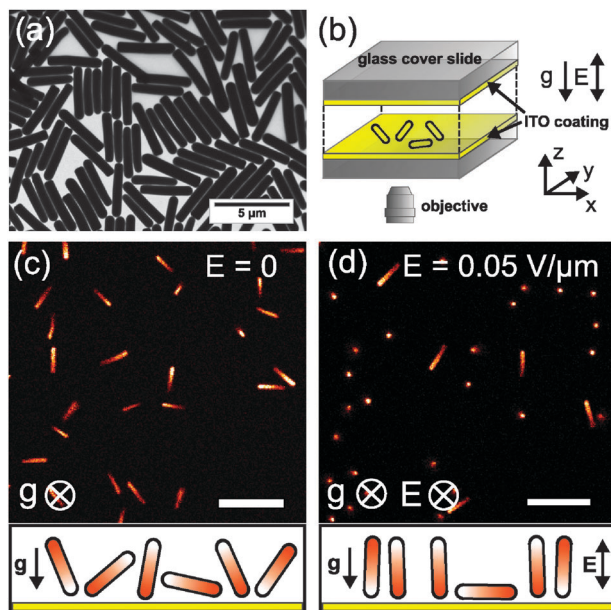
This journal is © the Owner Societies 2014

Phys. Chem. Chem. Phys., 2014, **16**, 22575–22582 | 22575

Fig. 1 Observation of bi-directional electric field alignment of colloidal silica rods. (a) Transmission electron microscopy (TEM) image of the silica rods with length $l = 3.6$ μm and diameter $d = 660$ nm. (b) Experimental setup. The height between the two indium tin oxide (ITO) coated glass slides was approximately 100 μm. (c and d) Confocal microscopy images of the particles suspended in an index-matching mixture of DMSO–water. The images were taken at the bottom of the sample, just above, and parallel with, the ITO electrode. The scale bars are 10 μm. Schematic drawings are shown at the bottom of the image. (c) Without an applied field, particles were randomly oriented. (d) When an electric field was applied ($E = 0.05$ V μm^{-1}), the majority of the particles aligned with the field direction, however, a significant number of particles was found to lie flat on the electrode. Notice that, due to the synthesis procedure, the particles had a gradient of fluorescent dye along their main axis,[16] as indicated in the schematics.

of the wires were wrapped around standard electronic wires that in turn were connected to the electrical setup.

For the electrical setup we used a function generator (Agilent 33120A) to generate a sinusoidal signal with a frequency of 1 MHz and an amplitude of 2.0 V (peak-to-peak). This signal was sent to the sample *via* a wide-band amplifier (Krohn-Hite, 7602 M) used to vary the field strength in the sample. We applied a high-frequency AC field to prevent polarization of the electric double layers of the particles[6] and the electrode. Because the electrodes are in direct contact with the suspension, the electric field strength is simply given by $E = \Delta V/d$ with ΔV the applied voltage and d the distance between the electrodes. The field strength is given in units V$_{RMS}$ μm^{-1}.

The fluorescent particles were imaged using an inverted confocal microscope (Leica SP2) and a $63\times/1.3$ oil immersion objective (Leica). We estimated the shortest distance between a silica rod and the conducting ITO plate by direct measurement of *xz* confocal microscopy images acquired in combined reflection and emission mode. The resulting distance of 176 ± 27 nm is close to twice the estimated thickness of the electric double layer of the particle ($\kappa^{-1} \approx 95$ nm).[17]

The confocal microscopy image in Fig. 1(c) shows that in the absence of an electric field, the particles formed a sediment on

the bottom electrode. The orientations of the particles were mainly parallel to the electrode, yet a distribution of other orientations existed due to thermal motion.[17] The particles of the first system (shown in the figure) had a gravitational length $l_g \approx 0.45$ μm, and those of the second system had $l_g \approx 0.7$ μm. These gravitational lengths are based on the particle dimensions that were obtained from TEM measurements.

When an electric field was applied ($E = 0.05$ V μm^{-1}), the majority of the particles aligned with the field direction; however, a significant number of particles (approximately 10%) were found to lie flat on the ITO electrode with an orientation perpendicular to the electric field, as shown in Fig. 1(d). These flat-lying particles were still able to perform (two dimensional) translational and rotational Brownian motion. This alignment effect was not observed when the electrodes were on the outside of the cell, *i.e.*, not in direct contact with the suspension. In that case, all the particles aligned as expected with the direction of the electric field.

3 Theory

The CDM models particles as built up out of Lorentz atoms (LAs) with polarizability α_0. These LAs do not necessarily reflect physical atoms, but rather "chunks" of matter that gain a dipole moment proportional (*via* α_0) to the locally experienced electric field. One can determine α_0 using the Clausius–Mossotti relation

$$\frac{\alpha_0 n}{\varepsilon_m} = \frac{3}{4\pi}\left(\frac{\varepsilon_p/\varepsilon_m - 1}{\varepsilon_p/\varepsilon_m + 2}\right), \tag{1}$$

where ε_m and ε_p are the dielectric constants of materials composing the medium and the particle, respectively, and n is the number density of LAs. We note that the Clausius–Mossotti relation may lead to negative as well as positive values for α_0.

Since a polarized LA will induce an additional electric field in its surroundings, each LA influences the local electric field felt by, and therefore the dipole moment of, all the other LAs. Within the CDM, the resulting many-body effects can be accounted for by large-matrix manipulation. We note that, within the CDM, these interatomic interactions are the reason that particles line up with electric fields: without interactions, the polarizability of the particle would be isotropic and hence the energy in the electric field would be independent of the orientation.

Starting off with a set of N LAs indexed by $i = 1, 2, \ldots, N$, we denote the location of atom i as $\mathbf{r}_i$ and its dipole moment as $\mathbf{p}_i$. We note that the electric field $\mathbf{E}_i$ experienced by atom i is given by the sum of the applied electric field and the electric field produced by all the other atoms:[24]

$$\mathbf{E}_i = \mathbf{E}_0 + \frac{1}{\varepsilon_m}\sum_{j=1}^{N}\mathbf{T}_{ij}\cdot\mathbf{p}_j,$$

where $\mathbf{T}_{ij}$ is the dipole–dipole tensor:

$$\mathbf{T}_{ij} = \begin{cases} \dfrac{\left(3\mathbf{r}_{ij}\mathbf{r}_{ij}\big/\left|\mathbf{r}_{ij}\right|^2 - \mathbf{I}\right)}{\left|\mathbf{r}_{ij}\right|^3} & \text{if } i \neq j, \\[4mm] 0 & \text{if } i = j, \end{cases}$$

where $\mathbf{r}_{ij} = \mathbf{r}_i - \mathbf{r}_j$. Substituting $\mathbf{E}_i = \mathbf{p}_i/\alpha_0$ and rearranging, we obtain the set of equations

$$\mathbf{p}_i - \frac{\alpha_0}{\varepsilon_m} \sum_{j=1}^{N} \mathbf{T}_{ij} \cdot \mathbf{p}_j = \alpha_0 \mathbf{E}_0. \qquad (2)$$

Note that the inclusion of ε_m into these equations constitutes a slight generalization with respect to earlier work on the CDM;[24–26,28] it represents the fact that the atoms are no longer "suspended" in a vacuum but in a medium with (relative) dielectric constant ε_m. The set of $\mathbf{p}_i$ can be obtained by numerically solving eqn (2); the potential energy U_E then follows from[25]

$$U_E = -\frac{1}{2} \sum_{i=1}^{N} \mathbf{p}_i \cdot \mathbf{E}_0. \qquad (3)$$

Here, the subscript "E" indicates that U_E is an electrostatic potential energy, present only if an external electric field is applied. If the external field $\mathbf{E}_0$ is spatially homogeneous, we can define a 3×3 cluster polarizability tensor $\boldsymbol{\alpha}_c$ such that

$$\sum_{i=1}^{N} \mathbf{p}_i = \boldsymbol{\alpha}_c \cdot \mathbf{E}_0,$$

and U_E can be rewritten as

$$U_E = -\tfrac{1}{2} \mathbf{E}_0 \cdot \boldsymbol{\alpha}_c \cdot \mathbf{E}_0.$$

Note that $\boldsymbol{\alpha}_c$ is symmetric if each LA has the same polarizability.[25] The cluster polarizability $\boldsymbol{\alpha}_c$ obtained from the CDM has, for several cluster shapes, been compared with predictions obtained using continuum electrostatics,[29–32] resulting in excellent agreement.[25]

The method of images[33] is a useful application of the uniqueness theorem of electrostatics, which states that a volume containing a given charge distribution and a given set of boundary conditions will have a uniquely defined electric field in its interior. This means that even if two systems are different outside a certain volume of interest, their electric fields inside this volume are identical if the boundary conditions on the surface of the volume and the charge distribution inside the volume are the same. Thus, if we encounter an electrostatic problem that seems difficult to solve, it is sometimes possible to solve a different, simpler problem instead, provided the same boundary conditions hold. The solution to the simpler problem will then also be the solution for the original, difficult problem.

The best-known example of the method of images is the problem of calculating the force on a point charge q a distance r from a conducting half-space at zero potential, as shown in Fig. 2(a). This problem may at first seem difficult to solve: since the field inside a conductor is zero, the conducting plate will accumulate a charge distribution at its surface to exactly compensate for the electric field due to the charge q and this charge distribution will subsequently exert a force on the point charge. We can solve the problem by looking at a different analogous setup. In a system where we have a charge q and a charge $-q$ separated by a distance $2r$ [Fig. 2(b)], the plane in the middle (i.e., a distance r from both charges) will have zero potential. Thus, in these two problems, the half-space that
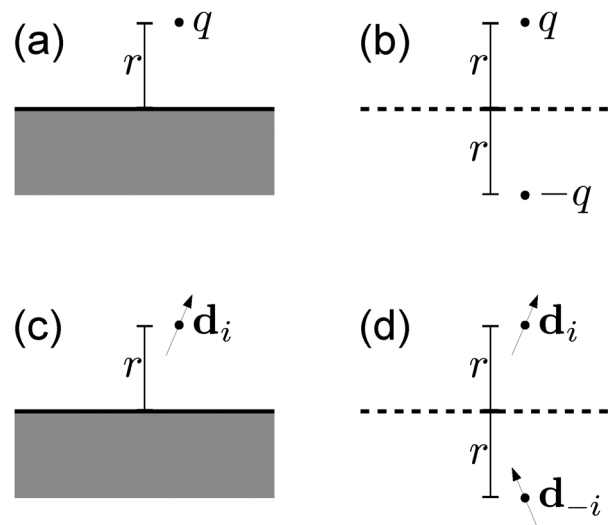

Fig. 2 Setup of the best-known example of the method of images: a point charge q is placed a distance r from a conducting half-space at zero potential (a). In the upper half-space, the resulting electric field is identical to the electric field in a setup where the conducting half-space is replaced by a single charge $-q$ placed exactly opposite to the original charge q (b), because the charge distribution and the boundary condition (zero potential at the dividing surface between the lower and upper half-space) are identical in both upper half-spaces. Since this reasoning can be applied to any number of charges, the interaction of an electric dipole $\mathbf{d}_i$ with a conducting half-space can be inferred a similar manner [panels (c) and (d)]. In these figures, the gray area is the conducting half-space and the horizontal line indicates the dividing plane between the upper and lower half-space and is at zero potential. It is dashed in panels (b) and (d) to indicate that there, it is not a physical surface.

contains the charge q has the same charge distribution (a single point charge q) and boundary condition (zero potential at its edge), hence the electric field in the half-space that contains q is the same in both problems. Thus, the force on the charge q in both problems would be $-q^2/4r^2$ (in CGS). Note that the solutions in the other half-space, i.e., the one that in the original problem contains the conductor and in the simplified problem contains charge $-q$, will not be the same.

It is not hard to see that we can apply the method of images to any charge distribution near a planar conductor. By placing image charges with the opposite sign and a mirrored position on the "conductor side" of the dividing plane, we ensure that the potential on the surface of the half-space of interest is zero. By picturing electric dipoles as a pair of charges of opposite sign a certain distance apart, we can work out what an image dipole should look like; explicitly, if the surface of the conductor is in the x–y plane and we have a point dipole $\mathbf{p}_i$ at location $\mathbf{r}_i$, the image dipole should have a dipole moment $\mathbf{p}_{-i}$ and location $\mathbf{r}_{-i}$ given by

$$\mathbf{p}_{-i} = \begin{pmatrix} -1 & 0 & 0 \\ 0 & -1 & 0 \\ 0 & 0 & 1 \end{pmatrix} \mathbf{p}_i, \quad \mathbf{r}_{-i} = \begin{pmatrix} 1 & 0 & 0 \\ 0 & 1 & 0 \\ 0 & 0 & -1 \end{pmatrix} \mathbf{r}_i. \qquad (4)$$

Here, we work in a fixed Cartesian (x, y, z) frame, and we adopted a notation where image dipoles are labeled by negative indices

$i = -1, -2, \ldots, -N$, such that each ("real") LA with index $i > 0$, dipole moment $\mathbf{p}_i$ and location $\mathbf{r}_i$ has an image dipole $\mathbf{p}_{-i}$ located at $\mathbf{r}_{-i}$. The method of images as applied to a dipole is pictured in Fig. 2(c) and (d). Proceeding to incorporate image dipoles in the CDM, we note that the "real" LAs still follow the relation $\mathbf{p}_i = \alpha_0 \mathbf{E}_i$, where $\mathbf{E}_i$ is the local electric field at $\mathbf{r}_i$, whereas the image dipoles gain their dipole moments not due to any external electric field: instead, their dipole moments are supposed to follow from $\mathbf{p}_i$ by eqn (4). For positive i, we now have that the electric field at site i is given by the external electric field plus the contributions from the real as well as the image dipoles:

$$\mathbf{E}_i = \mathbf{E}_0 + \frac{1}{\varepsilon_m} \sum_{j=-N}^{N} \mathbf{T}_{ij} \cdot \mathbf{p}_j \quad (i > 0),$$

where $\mathbf{T}_{ij}$ is the dipole–dipole tensor if $i \neq j$, and $\mathbf{T}_{ii} = 0$. We now plug in the proportionality of $\mathbf{p}_i$ with $\mathbf{E}_i$ and rearrange the terms,

$$\mathbf{p}_i - \frac{\alpha_0}{\varepsilon_m} \sum_{j=-N}^{N} \mathbf{T}_{ij} \cdot \mathbf{p}_j = \alpha_0 \mathbf{E}_0 \quad (i > 0),$$

and then eliminate the part of the sum that runs over negative indices:

$$\mathbf{p}_i - \frac{\alpha_0}{\varepsilon_m} \sum_{j=1}^{N} \mathbf{S}_{ij} \cdot \mathbf{p}_j = \alpha_0 \mathbf{E}_0 \quad (i > 0), \tag{5}$$

where

$$\mathbf{S}_{ij} \equiv \left[\mathbf{T}_{ij} + \mathbf{T}_{i,-j} \begin{pmatrix} -1 & 0 & 0 \\ 0 & -1 & 0 \\ 0 & 0 & 1 \end{pmatrix} \right]. \tag{6}$$

Note that $\mathbf{S}_{ii} \neq 0$, since in addition to $\mathbf{T}_{ii} = 0$, it has a contribution from $\mathbf{T}_{i,-i}$ which is nonvanishing. The structure of eqn (5) is, of course, identical to that of eqn (2) and it can thus be solved using exactly the same numerical methods, with the only difference that the 3×3 interaction matrices are somewhat modified. We calculate U_E via eqn (3), where we take note not to sum over negative indices. The interaction energy V_E between the cluster of Lorentz atoms and the conducting plate is obtained by subtracting from U_E the potential energy that would follow if there were no conducting plate present.

4 Results and discussion

A simple example system is one where a single LA with polarizability α_0 is a distance r away from a conducting half-space, and an electric field of strength E_0 is applied in the direction perpendicular to the surface of the half-space, defined here as the z-direction. The interaction energy of this problem can be found analytically. $\mathbf{S}_{ij}$ [as defined in eqn (6)] has to be calculated only for $i = j = 1$, meaning that its first term vanishes; the remaining term gives

$$\mathbf{S}_{11} = \frac{1}{8r^3} \begin{pmatrix} 1 & 0 & 0 \\ 0 & 1 & 0 \\ 0 & 0 & 2 \end{pmatrix}.$$

Inverting $\mathbf{I} - \alpha_0 \mathbf{S}_{11}/\varepsilon_m$ and multiplying by $\alpha_0 E_0 \hat{z}$ gives

$$\mathbf{p}_1 = \frac{\alpha_0 E_0}{1 - \alpha_0/4\varepsilon_m r^3} \hat{z}.$$

Taking the dot product with $-\frac{1}{2} E_0 \hat{z}$ gives us U_E, from which we subtract $U_E(r \to \infty) = -\frac{1}{2}\alpha_0 E_0^2$ to obtain the interaction energy

$$V_E = -\frac{1}{2} \frac{\alpha_0 E_0^2}{4\varepsilon_m r^3/\alpha_0 - 1}. \tag{7}$$

For large distances, the interaction energy goes as

$$V_E \simeq -\frac{1}{8} \frac{\alpha_0^2 E_0^2}{\varepsilon_m r^3} \quad (r^3/\alpha_0 \gg 1), \tag{8}$$

which is identical to the potential energy of a permanent dipole $\alpha_0 E_0 \hat{z}$ a distance r from a conducting plate; this energy is half that of two aligned permanent dipoles a distance $2r$ from each other because in our case the image dipole is induced by the real dipole, resulting in an extra factor $1/2$. From eqn (7), we see that at short distances, the interaction is either enhanced or reduced, depending on the sign of α_0. Also, in the case where $\alpha_0 > 0$, a polarization catastrophe occurs at distances $\varepsilon_m r^3/\alpha_0 < 1/4$ (or $r(\varepsilon_m/\alpha_0)^{1/3} \lesssim 0.63$) and the result is no longer valid. Both for positive and negative α_0, we plot $V_E/(\frac{1}{2}\alpha_0 E_0^2)$ as a function of the dimensionless distance $\tilde{r} = r|\varepsilon_m/\alpha_0|^{1/3}$, as well as the large-distance approximation eqn (8) (in which case the sign of α_0 is irrelevant), in Fig. 3.

We now turn our attention to the colloidal rods discussed in Section 2. We model a rod by placing LAs on a face-centered cubic (fcc) lattice and deleting any LAs that are located outside of a pre-defined spherocylinder shape, thus ending up with a cluster of LAs approximately spherocylindrical in shape. The cluster is then rotated and translated into the desired location and orientation with respect to the conductor surface. Note that the actual particle shape achieved this way will depend slightly on the lattice spacing chosen for the fcc lattice, because of the discrete nature of the lattice. In the following example, we chose a lattice spacing that (judging by eye) seemed to approximate the desired shape best. Additional numerical calculations (not shown here) using identical system parameters but different lattice spacings produce interaction energies that differ by up to 10% from the ones presented here. We will discuss here the example of a single rod of length $l = 3.6$ μm and width $d = 0.66$ μm, which we model as a cluster of 1413 LAs, spaced a distance $a_0 = l/36.39 \approx 98.9$ nm apart. To mimic the described experiments, we choose $\varepsilon_m = 50$ and $\varepsilon_p = 4.5$; plugging this into eqn (1), we find $\alpha_0 n/\varepsilon_m \approx -0.104$, which, assuming $n = \sqrt{2}/a_0^3$, leads to a dimensionless lattice constant of $a = a_0|\varepsilon_m/\alpha_0|^{1/3} \approx 2.39$. For comparison, we also show results for a rod with positive polarizability in the same solvent
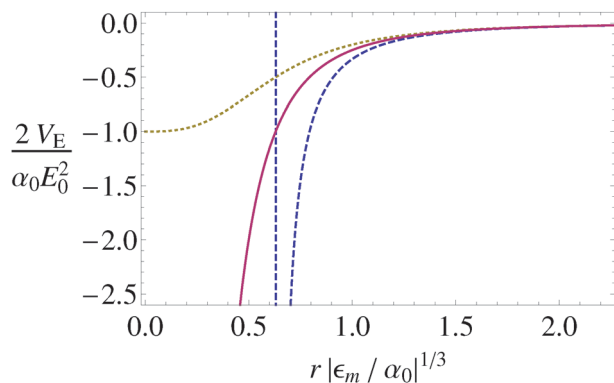
Fig. 3 The interaction energy $V_E/(\frac{1}{2}\alpha_0 E_0^2)$ of a Lorentz atom (LA) with polarizability α_0 with a conducting half-space at zero potential, as a function of the dimensionless distance $r|\varepsilon_m/\alpha_0|^{1/3}$ between the LA and the half-space, in the presence of an external electric field of magnitude E_0 and direction normal to the surface of the half-space. Plotted is the case $\alpha_0 > 0$ (blue dashed line), $\alpha_0 < 0$ (yellow dotted line), as well as the large-distance approximation (solid line), for which the sign of α_0 is irrelevant. The vertical dashed line at $r|\varepsilon_m/\alpha_0|^{1/3} \approx 0.63$ corresponds to the polarization catastrophe that occurs for positive polarizabilities.

(with $\varepsilon_m = 50$), with ε_p tuned such that $\alpha_0 n/\varepsilon_m \approx 0.104$ (this would be achieved for $\varepsilon_p \approx 166$). We place the tip of the rod at a certain distance r from the x–y plane and orient the rod such that it makes an angle θ with the z-axis. The setup is depicted in Fig. 4, from which it can be seen that the smallest allowed distance between the tip and the plate is $d/2$, suggesting that we define a gap length $h = r - d/2$, which vanishes if the rod is touching the plate. From the figure, we also see that the maximum allowed θ is $\pi/2$. We apply an electric field of $E_0 = 0.05$ V μm^{-1} in the z-direction, as in the experiments, and calculate the potential energy of the rod. We then subtract the energy that the rod would have if it were an infinite distance away from the plate and oriented in the direction of the electric field ($\theta = 0$) to obtain the interaction energy V_E of the rod with the plate. The results are plotted in Fig. 5 for several gap sizes h as a function of θ. Some numerical data are given in Table 1.

The orientation and distance dependence as well as the strength of the observed interaction energy shown in Fig. 5 are similar for positively and negatively polarizable rods. In both cases, the configuration where the rod is pointing in the $\hat{z}$-direction ($\theta = 0$) is energetically the most favorable, and for small distances a local minimum is observed at $\theta = \pi/2$, where the rod is oriented in the x–y plane.

Physically, this local minimum arises from a competition between dipoles lying head-to-toe and side-by-side with respect to each other. Fig. 6 depicts a simplified version of the situation for θ close to $\pi/2$. When in a horizontal position, the rod experiences, in addition to side-by-side interactions between its composing dipoles, significant attractions from the head-to-toe interactions between its composing dipoles and their image dipoles. When the rod is rotated slightly away from the horizontal position (i.e., to a somewhat lower θ), the side-by-side interactions are almost unaltered, while the dipoles in the tip being rotated away from the plate (the left tip in Fig. 6)
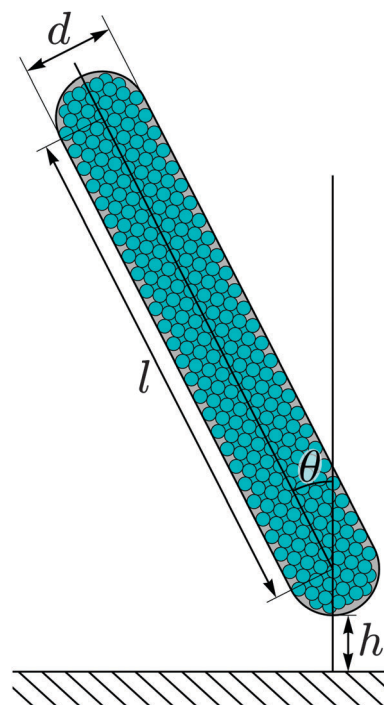

Fig. 4 Dissection of the setup for which the electrostatic interaction energy is calculated and plotted in Fig. 5. A spherocylindrical rod consisting of 1413 LAs is positioned near a conducting half-space at zero potential, while an electric field $\boldsymbol{E}_0$ is applied normal to the surface of the half-space. The rod's position and orientation are defined by the distance h between its tip and the surface of the conducting half-space and the angle θ between the director of the rod and the line normal to the surface of the half-space.

experience much less attractive interaction with their image dipoles because of the increased distance. Mathematically speaking, the rod's "self-energy" (i.e. the energy of the rod if no surroundings are present except an external electric field) goes (using our current definitions) as[26] $\propto \sin^2\theta$, a nearly constant function near $\theta = \pi/2$, while the interaction between the rod dipoles and their images is more complicated but can be expected to be akin to an inverse power law in $l\cos\theta$. Near $\theta = \pi/2$, the former contributes only a constant term, while the latter contributes a negative term that quickly becomes less negative as θ decreases. The result is that V_E increases when θ is lowered from $\pi/2$. One tip of the rod (the right tip in Fig. 6), however, is always kept at a constant distance to the plate, such that additional rotation towards even lower θ will have decreased effect on the image attractions, while the effects on the side-by-side interactions become more and more appreciable. Mathematically, this corresponds to the $\propto \sin^2\theta$ self-energy of the rod becoming less constant, and the image interaction term becoming more constant because the parts of the rod whose positions depend most on θ have already been rotated away from the plate, such that their interaction contribution has dwindled. Eventually, the $\propto \sin^2\theta$ self-energy of the rod (which decreases as θ decreases) overcomes the effect of decreased image attraction, resulting in a reversal of the trend in V_E (i.e., V_E will start to decrease as θ decreases). The angle where this reversal occurs is the θ-location of the
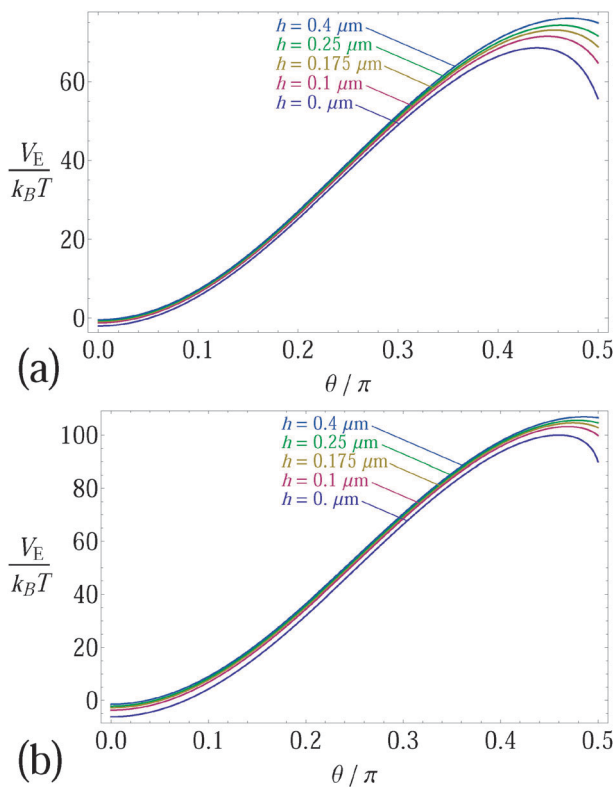
Fig. 5 Interaction energy between a rod suspended in a medium with $\varepsilon_m = 50$ and a conducting half-space (as depicted in Fig. 4) as a function of the angle θ between the rod director and the line normal to the surface of the half-space, for gap lengths $h = 0$ μm, 0.1 μm, 0.175 μm, 0.25 μm and 0.4 μm. Two cases are depicted, namely (a) a negatively polarizable rod with dielectric constant $\varepsilon_p = 4.5$ and (b) a positively polarizable rod with $\varepsilon_p \approx 166$. In both cases, the applied electric field strength is $E_0 = 50$ V μm^{-1} and the temperature is $T = 293$ K.

Table 1 Relevant numerical data associated with the graphs in Fig. 5. For each gap length h, the angle θ_0 at which the maximum occurs is given, as well as the depth Δ of the potential energy well at $\theta = \pi/2$, in units of $k_B T$ where $T = 293$ K. Table (a) pertains to negatively polarizable rods ($\varepsilon_p = 4.5$) and (b) to positively polarizable rods ($\varepsilon_p \approx 166$)

h (μm)	θ_0/π	$\Delta/k_B T$
(a)		
0.0	0.439	12.80
0.1	0.450	6.73
0.175	0.456	4.23
0.25	0.462	2.70
0.4	0.472	1.16
(b)		
0.0	0.460	10.07
0.1	0.469	3.32
0.175	0.474	1.76
0.25	0.479	0.99
0.4	0.486	0.34

maximum of V_E, which we shall denote by θ_0. The rest of the graph (i.e., $\theta < \theta_0$) is dominated by the interaction between rod dipoles, i.e., the $\sin^2 \theta$-dependence; in this region ($\theta < \theta_0$), the interaction between rod dipoles and their image dipoles is nearly constant since the only significant contribution to that interaction
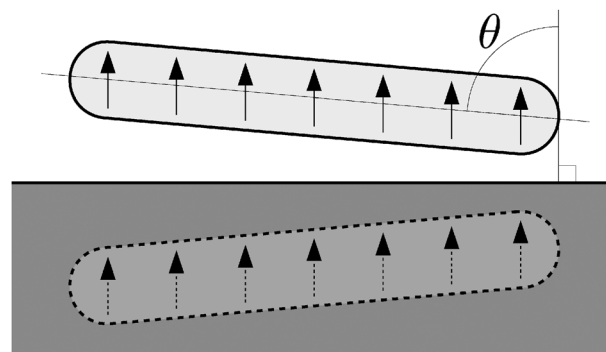

Fig. 6 Simplified depiction of the physical situation discussed in the text: a rod is close to an electrode and near horizontal orientation. For the purposes of the physical (qualitative) discussion, we only need to consider a low number of composing dipoles (represented here as arrows). These dipoles interact among each other as well as with the electrode. Pictured inside the conductor is also the image of the rod: the interaction of the real rod with the electrode is identical to the interaction of its composing dipoles with the image dipoles.

comes from the tip closest to the plate (the right tip in Fig. 6), which does not change position with changing θ.

In the previous paragraph (as well as elsewhere in this paper) we have discussed the physics in terms of interaction between the rod dipoles and their images. It should be emphasized that this is slightly inaccurate: it would be correct to say that the interaction occurs between the dipoles and the electrode, and is equal to the interaction that would occur in an analogous setup where the electrode is replaced by a half-space that is empty except for image dipoles placed at the appropriate locations.

Both θ_0 and the depth of the local minimum at $\theta = \pi/2$, depend on the distance to the plate; for negatively polarizable rods at contact it is located at $\theta_0 \approx 0.439\pi$ and for positively polarizable ones it is found at $\theta_0 \approx 0.460\pi$. The local minimum at contact is about $12.8 k_B T$ deep in the case of negatively polarizable rods, and $10.07 k_B T$ in the case of positively polarizable rods. In the experiments, the rods never physically touch the plate but rather "float" at a certain distance above it due to a screened-coulomb interaction with the plate. This minimum gap between the rod and the plate has been determined to be roughly 175 nm; in that case, the depth of the local minimum is only $4.23 k_B T$ and $1.76 k_B T$ for negatively and positively polarizable rods, respectively, and the maximum has shifted to (slightly) higher θ, being located at 0.456π and 0.474π for negatively and positively polarizable rods, respectively. For even larger gaps the local minimum quickly becomes negligible compared to $k_B T$ (for the chosen electric field strength) and the maximum shifts to an even higher θ. We thus see that rods at contact are retained in the local minimum (the horizontal, "lying-down" position) relatively easily, but that in the more realistic case where the gap is $h = 175$ nm, a positively polarizable rod cannot be kept in the horizontal position for a long time. A negatively polarizable rod can be retained somewhat longer but will eventually overcome the potential energy barrier as well, and will then align (vertically) with the electric field.

22580 | Phys. Chem. Chem. Phys., 2014, 16, 22575–22582

This journal is © the Owner Societies 2014

From the graphs, we also see that an applied electric field will pull the rods close to the plate either towards a horizontal or vertical position, depending on which orientation they start with. Roughly speaking, for rods at the minimum distance of 175 nm the fraction of rods ending up in a horizontal position can be expected to be the fraction of rods starting out with an orientation such that $\theta > \theta_0$ (where θ_0, as introduced earlier, is the orientation where the interaction energy exhibits a maximum at fixed h). Assuming a completely random starting configuration with an isotropic distribution of the orientations of rods, this fraction is simply the fractional surface area of a "belt" representing $\theta > \theta_0$ around the equator of a unit hemisphere, i.e., $f(\theta_0) = \int_{\theta_0}^{\pi/2} \mathrm{d}\theta \sin\theta = \cos\theta_0$, which, for $\theta_0 \approx 0.456\pi$, amounts to $f \approx 0.14$. This estimate is comparable in magnitude to the fractions of horizontal particles observed in the experiments.

We conclude that, qualitatively, the theoretical results as presented above, including the existence of a local minimum at the horizontal ("lying-down") position and a global one at the vertical ("standing-up") position, as well as the magnitude of interaction energies observed, agree well with experiments. We are therefore confident that our theory provides a valid qualitative explanation for the experimental observations. There is, however, a number of factors that likely impede the quantitative accuracy of the theory, apart from the aforementioned effects due to the arbitrariness when choosing an fcc lattice spacing for modeling the rod, which we will now list.

An experimental complication is that the local minimum at the horizontal position is shallow (smaller than $10k_BT$ except at contact), so that the percentage of horizontally lying particles measured in an experiment depends on how much time has passed between turning on the electric field and imaging the sample.

A number of complications were ignored when calculating $f(\theta_0)$. First of all, the assumption of a random, isotropic starting configuration is problematic, because the mass of the rods will influence the statistics of the configuration (heavier rods will tend to lie horizontally more often). We note here that the mass of the rods is only expected to be important for the starting configuration: once the field is switched on, the rods are clearly observed to either lie horizontally or stand vertically, indicating that the electrostatic potential dominates the dynamics. The presence of a wall might in some cases also influence the statistics through excluded volume interactions. A second ignored complication when calculating $f(\theta_0)$ is that its reasoning does not hold for rods that do not start out at the minimum distance of 175 nm. Once the field is turned on, rods that are far enough from the plate will probably first rotate to an aligned (vertical) position and then arrive at the plate, thus lowering the percentage of horizontally lying rods. We note here that, interestingly, rods that do *not* have time to rotate to a standing-up position may end up lying down even if, initially, their orientation was such that $\theta < \theta_0$. This is because, while translating towards the plate, the location of θ_0 shifts significantly to lower values. For instance, a negatively polarizable rod starting at $h = 0.4$ mm, with orientation $\theta = 0.46\pi$ (which is below θ_0 for this h)

might translate towards smaller h before it rotates significantly, shifting its θ_0 to values below its θ, and hence ending up in the lying down position even though it started out with $\theta < \theta_0$.

Although our theory is capable of dealing with interparticle electric field-induced dipolar interactions, we have chosen to consider only the interaction between a single particle and its image in this paper, thus ignoring interparticle interactions. The presence of other particles will influence the interaction a rod has with its image, but this effect is probably minor. More significant effects are, for dense systems, excluded-volume interactions and, for all but the most dilute systems, the aforementioned interparticle electric field-induced dipolar interactions. For a pair of rods lying head-to-toe, parallel to the electric field and far away from the conducting half-space, the interaction energy at the assumed minimum gap length of 175 nm and for the aforementioned experimental parameters amounts to about $-2.6k_BT$ for negatively, and $-7.8k_BT$ for positively polarizable rods. A comparison with the values quoted in Table 1 thus reveals that, for negatively polarizable rods, dipolar interactions can have an appreciable influence on the system, while for positively polarizable rods, dipolar interactions will dominate and the system will exhibit string formation rather than rods lying flat on the electrode. To get an estimate of the percentage of horizontally lying rods predicted by our theory better than the rough sketch given above, simulations will have to be performed taking into account the various complications listed.

The magnitude of the interaction energy depends quadratically on the electric field strength, such that lower electric field strengths create more shallow local potential minima, while higher field strengths will make the minima deeper. This means that stronger electric fields will be better able to retain rods in the horizontal position. The aforementioned time-dependence arising from the shallow minimum at horizontal positions, could be eliminated in this way. We note here that experimentally, we have observed that at high field strengths, not only do the rods either stand up or lie down, they also tend to form structures where several rods are standing on top of a single rod that lies horizontally on the electrode. In Fig. 7 we
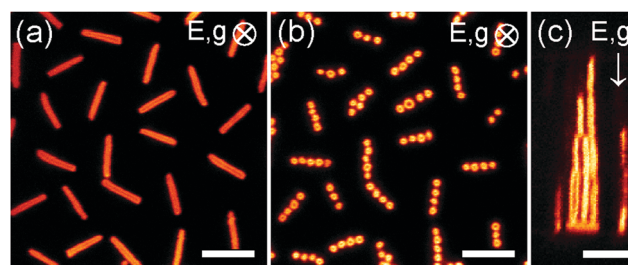

Fig. 7 Rods with length $l = 3.3$ μm and diameter $d = 550$ nm in an electric field $E = 0.5$ V μm^{-1}. The spacing between the electrodes was approximately 15 μm. (a) Rods on the bottom electrode oriented parallel to the electrode surface (flat). The rods still performed (in plane) rotational and translation motion. (b) First layer of rods standing on top of the flat rods. (c) A side-view shows that several layers of rods were positioned on top of the flat ones. The scale bars are 5 μm.

This journal is © the Owner Societies 2014

Phys. Chem. Chem. Phys., 2014, **16**, 22575–22582 | **22581**

show an example of such a configuration for field strength $E = 0.5$ V μm^{-1}. To explain this behavior, interactions between the rods have to be taken into account, which is beyond the goals of the present paper. The experimental system that was highlighted in this paper (*e.g.*, Fig. 1(d), where $E = 0.05$ V μm^{-1} was used) did not exhibit such stacked structures, and the presentation and explanation for the stacking behavior as seen in Fig. 7 will be left for further study.

Acknowledgements

References

1 A. Blaaderen, M. Dijkstra, R. Roij, A. Imhof, M. Kamp, B. W. Kwaadgras, T. Vissers and B. Liu, *Eur. Phys. J.: Spec. Top.*, 2013, **222**, 2895–2909.

2 K. Bubke, H. Gnewuch, M. Hempstead, J. Hammer and M. L. H. Green, *Appl. Phys. Lett.*, 1997, **71**, 1906–1908.

3 A. F. Demirörs, P. M. Johnson, C. M. van Kats, A. van Blaaderen and A. Imhof, *Langmuir*, 2010, **26**, 14466–14471.

4 P. A. Smith, C. D. Nordquist, T. N. Jackson, T. S. Mayer, B. R. Martin, J. Mbindyo and T. E. Mallouk, *Appl. Phys. Lett.*, 2000, **77**, 1399–1401.

5 K. M. Ryan, A. Mastroianni, K. A. Stancil, H. Liu and A. P. Alivisatos, *Nano Lett.*, 2006, **6**, 1479–1482.

6 A. Yethiraj and A. van Blaaderen, *Nature*, 2003, **421**, 513–517.

7 H. R. Vutukuri, J. Stiefelhagen, T. Vissers, A. Imhof and A. van Blaaderen, *Adv. Mater.*, 2012, **24**, 412–416.

8 K. Kang and J. K. G. Dhont, *Europhys. Lett.*, 2008, **84**, 14005.

9 U. Dassanayake, S. Fraden and A. van Blaaderen, *J. Chem. Phys.*, 2000, **112**, 3851–3858.

10 A.-P. Hynninen and M. Dijkstra, *Phys. Rev. Lett.*, 2005, **94**, 138303.

11 A.-P. Hynninen and M. Dijkstra, *Phys. Rev. E: Stat., Nonlinear, Soft Matter Phys.*, 2005, **72**, 051402.

12 F. Smallenburg and M. Dijkstra, *J. Chem. Phys.*, 2010, **132**, 204508.

13 F. Smallenburg, H. R. Vutukuri, A. Imhof, A. van Blaaderen and M. Dijkstra, *J. Phys.: Condens. Matter*, 2012, **24**, 464113.

14 D. Levesque and J.-J. Weis, *Mol. Phys.*, 2011, **109**, 2747–2756.

15 A. Kuijk, A. van Blaaderen and A. Imhof, *J. Am. Chem. Soc.*, 2011, **133**, 2346–2349.

16 A. Kuijk, A. Imhof, M. H. W. Verkuijlen, T. H. Besseling, E. R. H. van Eck and A. van Blaaderen, *Part. Part. Syst. Charact.*, 2014, **31**, 706–713.

17 A. Kuijk, D. V. Byelov, A. V. Petukhov, A. van Blaaderen and A. Imhof, *Faraday Discuss.*, 2012, **159**, 181–199.

18 A. Kuijk, T. Troppenz, L. Filion, A. Imhof, R. van Roij, M. Dijkstra and A. van Blaaderen, *Soft Matter*, 2014, **10**, 6249–6255.

19 T. Troppenz, A. Kuijk, A. Imhof, A. van Blaaderen, M. Dijkstra and R. van Roij, manuscript in preparation.

20 M. Renne and B. Nijboer, *Chem. Phys. Lett.*, 1967, **1**, 317–320.

21 B. Nijboer and M. Renne, *Chem. Phys. Lett.*, 1968, **2**, 35–38.

22 M. W. Cole and D. Velegol, *Mol. Phys.*, 2008, **106**, 1587–1596.

23 H.-Y. Kim, J. O. Sofo, D. Velegol, M. W. Cole and A. A. Lucas, *J. Chem. Phys.*, 2006, **124**, 074504.

24 H.-Y. Kim, J. O. Sofo, D. Velegol, M. W. Cole and G. Mukhopadhyay, *Phys. Rev. A: At., Mol., Opt. Phys.*, 2005, **72**, 053201.

25 B. W. Kwaadgras, M. Verdult, M. Dijkstra and R. van Roij, *J. Chem. Phys.*, 2011, **135**, 134105.

26 B. W. Kwaadgras, M. Dijkstra and R. van Roij, *J. Chem. Phys.*, 2012, **136**, 131102.

27 B. W. Kwaadgras, M. W. J. Verdult, M. Dijkstra and R. van Roij, *J. Chem. Phys.*, 2013, **138**, 104308.

28 B. W. Kwaadgras, R. van Roij and M. Dijkstra, *J. Chem. Phys.*, 2014, **140**, 154901.

29 A. Sihvola, *J. Nanomater.*, 2007, **2007**, 45090.

30 A. Sihvola, P. Yla-Oijala, S. Jarvenpaa and J. Avelin, *IEEE Trans. Antennas Propag.*, 2004, **52**, 2226–2233.

31 M. Pitkonen, *J. Appl. Phys.*, 2008, **103**, 104910.

32 M. Pitkonen, *J. Math. Phys.*, 2006, **47**, 102901.

33 J. D. Jackson, *Classical Electrodynamics*, John Wiley & Sons, Inc., 3rd edn, 1999.